Available online at www.sciencedirect.com
ScienceDirect
Dyes and Pigments 77 (2008) 204–209
DYES and PIGMENTS
www.elsevier.com/locate/dyepig

Photocatalytic degradation of C.I. Acid Orange 52 in the presence of Zn-doped TiO_2 prepared by a stearic acid gel method

Cheng Chen [a], Zhuyi Wang [a], Shengping Ruan [b], Bo Zou [a], Meng Zhao [a], Fengqing Wu [a,*]

[a] College of Chemistry, Jilin University, Changchun 130023, China
[b] College of Electronic Science and Engineering, Jilin University, Changchun 130023, China

Received 27 January 2007; received in revised form 3 May 2007; accepted 10 May 2007
Available online 24 May 2007

Abstract

Zn-doped TiO_2 nanocrystals were prepared using a stearic acid gel method and were characterized by X-ray powder diffraction, scanning electron microscopy (SEM), Brunauer–Emmett–Teller (BET) surface area and UV–vis diffuse reflectance spectroscopy. When the nanocrystals were used for the photodegradation of methyl orange in water under UV irradiation, it was found that the 0.1 at% Zn-doped TiO_2 nanocrystalline catalyst exhibited greater photodegradation than TiO_2 nanocrystals which had been prepared using a sol–gel method as well as the international reference material, P25 titania. This was rationalized in terms of the role of the Zn dopant in the TiO_2 nanocrystals and BET surface area. Liquid chromatography/mass spectrometry (LC/MS) analysis confirmed that the dye was completely degraded after 30 min using the 0.1% Zn-doped TiO_2 nanocrystals.

Keywords: TiO_2; Zn-doped; Stearic acid gel method; Photocatalysis; Degradation; Methyl orange

1. Introduction

Dye pollutants are important sources of environmental contamination. Textile wastewater contains a considerable amount of unfixed dyes, many of which are azo compounds [1] which can be effectively removed by photocatalysis with semiconductor catalysts of which, nano-TiO_2 is widely utilized due to its outstanding stability, inexpensiveness, lack of toxicity and strong photoactivity [2–10].

To enhance its photoactivity, TiO_2 is often doped with various metal ions and oxides such as Zn, Pt, Pd, Au, Ag, Cu, WO_3, V_2O_5, etc. [11–17]. The dopants act as charge separators of photoinduced electron–hole pairs and it is proposed that, after excitation, the electron migrates to the metal where it becomes trapped and electron–hole recombination is suppressed [18]. The photoactivity of TiO_2 is not only affected by the separation and lifetime of the photoproduced electron–hole pairs, but also relates to the bulk, crystal phase, surface area and the distribution of photoactive components. Kasuga et al. synthesized nanotube TiO_2 of very large surface area, but low photoactivity [19] while Madras et al. prepared metal ion substituted anatase titania by a solution combustion method [18] and zinc was used to dope pure anatase or pure rutile titania [20]; sol–gel has been used as a common process to produce pure or doped titania [21–23].

In this work, a stearic acid gel method was used to prepare Zn-doped TiO_2 nanocrystals and the ability of the Zn-doped TiO_2 to degrade methyl orange (C.I. Acid Orange 52), chosen as a representative of an azo dye, was investigated as a function of the concentration of zinc, BET surface area and calcination temperature. The results were compared with those obtained using TiO_2 nanocrystals prepared using a sol–gel method and a commercial sample, P25.

* Corresponding author. Tel.: +86 431 85168397.
E-mail address: fqwu@mail.jlu.edu.cn (F. Wu).

0143-7208/$ - see front matter © 2007 Published by Elsevier Ltd.
doi:10.1016/j.dyepig.2007.05.003

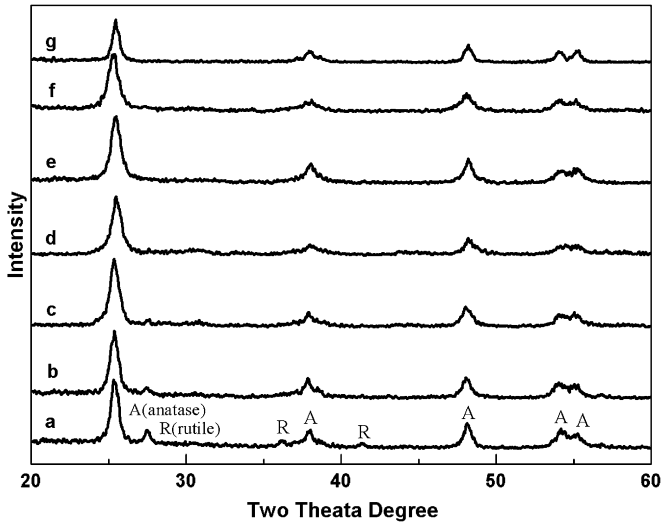

Fig. 1. XRD patterns of Zn/TiO_2 nanocrystals calcined at 450 °C: (a) undoped $TiO_{2\ ste}$; (b) 0.05% $Zn/TiO_{2\ ste}$; (c) 0.1% $Zn/TiO_{2\ ste}$; (d) 0.3% $Zn/TiO_{2\ ste}$; (e) 0.5% $Zn/TiO_{2\ ste}$; (f) 1.0% $Zn/TiO_{2\ ste}$; (g) 0.1% $Zn/TiO_{2\ sol}$.

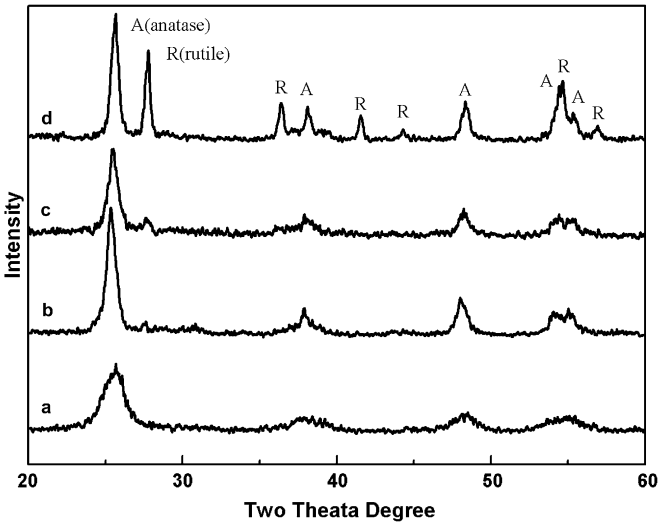

Fig. 2. XRD patterns of 0.1% $Zn/TiO_{2\ ste}$ nanocrystals calcined at various temperatures: (a) 400 °C; (b) 450 °C; (c) 500 °C; (d) 600 °C.

2. Experimental section

2.1. Catalyst preparation

2.1.1. Stearic acid gel method

Doped TiO_2 nanocrystals were prepared by adding titanium tetraisopropoxide (CP, 2.5 ml) to melting stearic acid (AR, 10 g) with vigorous stirring at 70 °C followed by the addition of zinc acetate. The molar ratios of Zn^{2+}/Ti^{4+} were 0.05%, 0.1%, 0.3%, 0.5%, and 1.0%. After 2 h, the mixture was cooled in cold water, then heated in air at 300 °C and subsequently calcined at 400 °C, 450 °C, 500 °C, and 600 °C for 2 h.

2.1.2. Sol–gel method

The preparation of the doped TiO_2 nanocrystals by the sol–gel method followed the work of Sun [21]. Titanium tetraisopropoxide (CP, 10 ml) was mixed with anhydrous ethanol (CP, 40 ml) and the mixture was then added dropwise into a mixture of water (10 ml), anhydrous ethanol (CP, 10 ml), 70% HNO_3 (CP, 2 ml), and zinc acetate (CP). The ensuing reaction mixture was stirred at room temperature for 3 h until a yellow coloured transparent sol was obtained. After drying at room temperature, the yellow solid was calcined at 450 °C for 2 h.

A commercial sample of the internationally used reference material P25 was obtained from Degussa.

2.2. Characterization

X-ray powder diffraction (XRD) analysis was carried out using a Shimadzu LabX XRD-6000 and scanning electron microscopy (SEM) studies were performed with a JEOL JSM-6700F. Specific surface areas were measured by the BET method employing a nitrogen adsorption–desorption analyzer (Quantachrome AUTOSORB-1C). UV–vis diffuse reflectance spectra analysis was performed using a Perkin–Elmer Lambda 20.

2.3. Photochemical reaction

The photodegradation of the dye (20 mg/l) was carried out in a jacketed column quartz reactor (700 ml). A high pressure mercury lamp (300 W) was placed in a quartz tube which was then placed inside the reactor. Using a catalyst concentration of 1 g/l, reaction was carried out at 25 °C, maintained by circulating water in the annulus of the reactor. Aliquots (2 ml) of the solutions were collected at regular intervals for subsequent analysis by mass spectrometry.

3. Results and discussions

3.1. XRD

Fig. 1 shows the XRD patterns of Zn-doped TiO_2 nanocrystals calcined at 450 °C. Letters in the subscript indicate the synthetic methods of samples, i.e. $TiO_{2\ ste}$ stands for TiO_2 prepared by the stearic acid gel method, $TiO_{2\ sol}$ for TiO_2 prepared by the sol–gel method and Zn/TiO_2 represents Zn-doped TiO_2. The characteristic peaks of the rutile and anatase forms are indicated in Fig. 1. Comparing the characteristic

Table 1
The grain size and the intensity ratio (I_R/I_A) of Zn/TiO_2 nanocrystals calcined at 450 °C as determined from XRD patterns in Fig. 1

Dopant concentration (%)	0_{ste}	0.05_{ste}	0.1_{ste}	0.3_{ste}	0.5_{ste}	1.0_{ste}	0.1_{sol}
Grain size (nm)	11.8	10.8	10.9	10.3	10.8	10.2	14.4
I_R/I_A (%)	11	11	10	5	0	0	0

Table 2
The grain size and the intensity ratio (I_R/I_A) of 0.1% $Zn/TiO_{2\ ste}$ nanocrystals calcined at various temperatures as determined from XRD patterns in Fig. 2

Calcination temperature (°C)	400	450	500	600
Grain size (nm)	6.1	10.9	15.9	19.4
I_R/I_A (%)	0	10	16	68

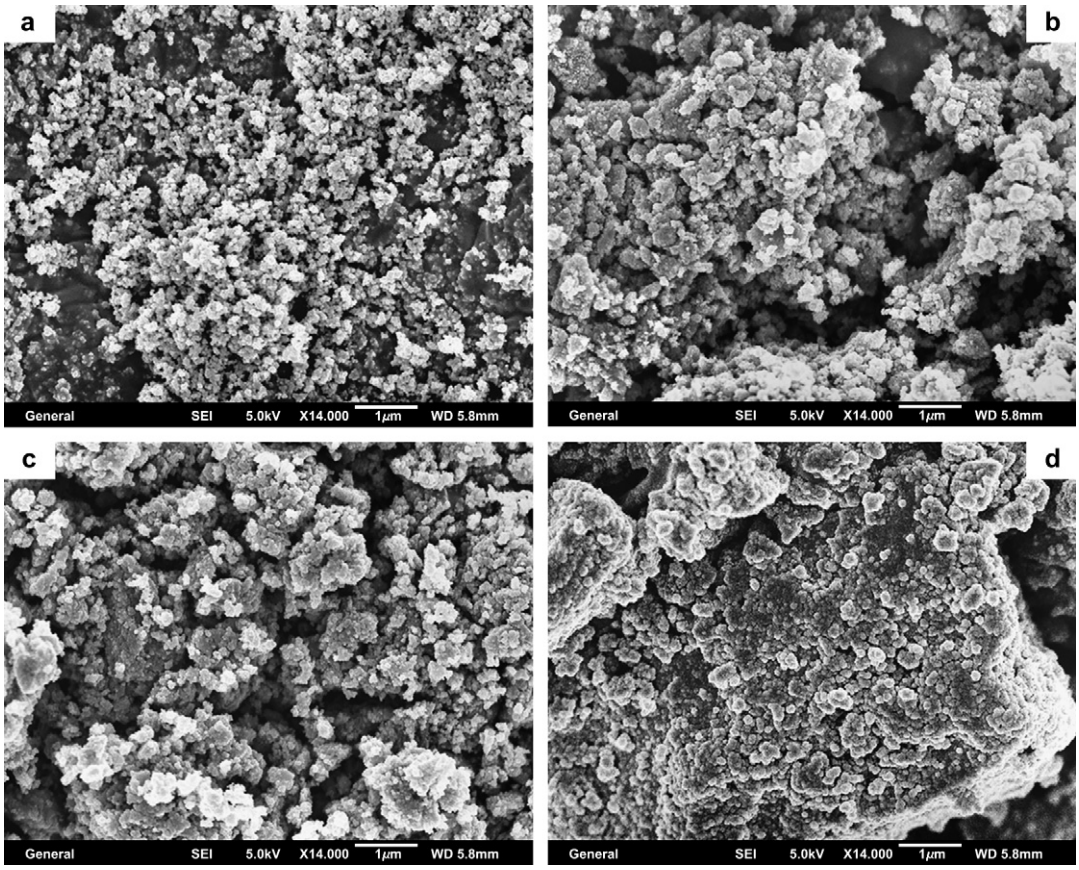

Fig. 3. SEM images of (a) P25; (b) $TiO_{2\ ste}$ calcined at 450 °C; (c) 0.1% $Zn/TiO_{2\ ste}$ calcined at 450 °C; (d) 0.1% $Zn/TiO_{2\ sol}$ calcined at 450 °C.

peak intensities of the rutile (I_R, 27.4°) and the anatase (I_A, 25.4°) forms reveals that the intensity ratio (I_R/I_A) of $Zn/TiO_{2\ ste}$ was lower than that of undoped $TiO_{2\ ste}$, indicating that the doped zinc inhibited the transformation of the anatase phase to the rutile phase. Table 1 shows the grain sizes of the samples, determined using the Scherrer equation; the amount of doped zinc had no influence on the grain sizes of the samples prepared by the stearic acid gel method.

Fig. 2 shows the XRD patterns of 0.1% $Zn/TiO_{2\ ste}$ nanocrystals calcined at various temperatures. It was found that the intensity ratio (I_R/I_A) increased with increasing calcination temperature, indicating that the anatase form was gradually transformed to the rutile phase. The grain sizes and the intensity ratios (I_R/I_A) for 0.1% $Zn/TiO_{2\ ste}$ are shown in Table 2. As calcination temperature increased, the grain size increased and the proportion of the rutile phase also increased, indicating that the higher calcination temperature favoured the formation of larger crystals and the rutile phase TiO_2.

3.2. SEM

The SEM images of various samples are shown in Fig. 3. $TiO_{2\ ste}$ and $Zn/TiO_{2\ ste}$ (Fig. 3b and c) exhibited smaller crystallite agglomeration than $Zn/TiO_{2\ sol}$ (Fig. 3d). This can be explained as follows: when the samples were prepared by the stearic acid gel method, $Ti(OC_4H_9)_4$ was dispersed in stearic acid, thus preventing the particles from agglomerating; hence, smaller crystallite agglomerations were formed.

3.3. BET

Table 3 shows the BET surface areas of the commercial P25 and TiO_2-based nanocrystals calcined at 450 °C; the samples prepared by the stearic acid gel method showed much higher BET surface area.

3.4. UV–vis

The absorption spectra of Zn/TiO_2 nanocrystals calcined at 450 °C are shown in Fig. 4 from which it is evident that the amount of zinc dopant did not have a significant effect on the absorption band of Zn/TiO_2 prepared by the stearic acid gel method. The absorption bands of 0.1% $Zn/TiO_{2\ ste}$ and 0.1% $Zn/TiO_{2\ sol}$ were similar.

However, Fig. 5 reveals that the absorption band was influenced by calcination temperature. The band-gap energy of the

Table 3
BET surface areas of P25 and TiO_2-based nanocrystals calcined at 450 °C

Sample	P25	$TiO_{2\ ste}$	0.1% $Zn/TiO_{2\ ste}$	$TiO_{2\ sol}$	0.1% $Zn/TiO_{2\ sol}$
Surface area (m^2/g)	53.61	91.25	152.0	39.75	27.34

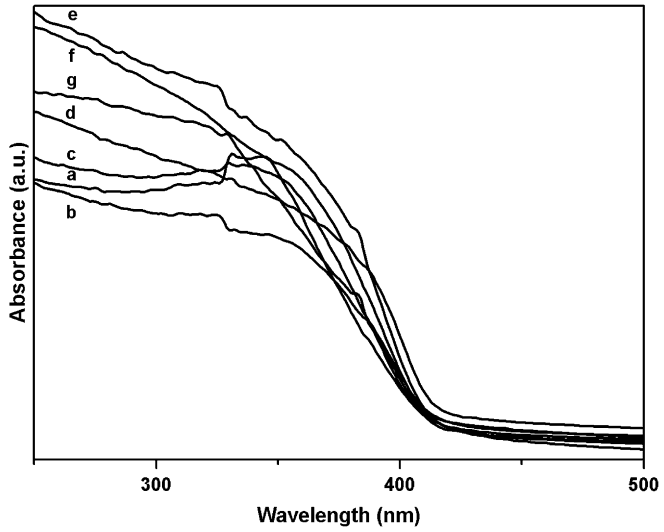

Fig. 4. UV absorption spectra of Zn/TiO_2 calcined at 450 °C: (a) undoped $TiO_{2\ ste}$; (b) 0.05% $Zn/TiO_{2\ ste}$; (c) 0.1% $Zn/TiO_{2\ ste}$; (d) 0.3% $Zn/TiO_{2\ ste}$; (e) 0.5% $Zn/TiO_{2\ ste}$; (f) 1.0% $Zn/TiO_{2\ ste}$; (g) 0.1% $Zn/TiO_{2\ sol}$.

anatase and the rutile forms of titania are 3.2 eV and 3.0 eV, respectively. As the absorption band of the rutile phase shifts to longer wavelength, the observed absorption (curve d) at higher wavelength may be ascribed to the increasing proportion of the rutile phase, which is consistent with the data shown in Table 2.

3.5. Photoreactivity experiments

The degradation profiles for $Zn/TiO_{2\ ste}$ nanocrystals calcined at 450 °C are shown in Fig. 6. The 0.1% $Zn/TiO_{2\ ste}$ nanocrystals exhibited the best photodegradation of the dye. The photoactivity of the samples decreased when the concentration of zinc was less or greater than 0.1%, indicating that there was an optimal dosage of zinc. The effect of metal ion dopants on the photoactivity of many materials has been widely studied. Different hypotheses have been proposed to explain their roles [1,11,24–27]. In our case, no obvious shift in the absorption band edges was observed for the samples as shown in Fig. 4, indicating that the effect of absorption band edge on photoactivity can be ignored. At zinc concentrations below the optimal level, the observed improvement in photoactivity that accompanied zinc doping can be explained by the fact that the zinc promotes the separation of electron–hole pairs in titania, since the doped ions can act as separators of electron–hole pairs. At zinc concentration above the optimal level, the doped zinc mainly acts as a charge carrier recombination center; recombination of the electron–hole pair increases with dopant concentration because the average distance between trap sites decreases with increasing the number of dopant molecules confined within a particle [11]. Thus, the appearance of an optimal dopant concentration is a result of the delicate balance of an increase in trap sites leading to efficient trapping and fewer trapped carriers leading to longer lifetimes for interfacial charge transfer.

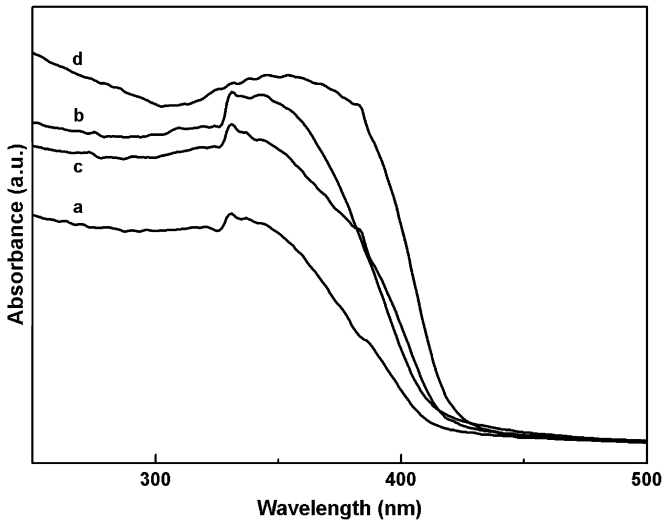

Fig. 5. UV absorption spectra of 0.1% $Zn/TiO_{2\ ste}$ calcined at various temperatures: (a) 400 °C; (b) 450 °C; (c) 500 °C; (d) 600 °C.

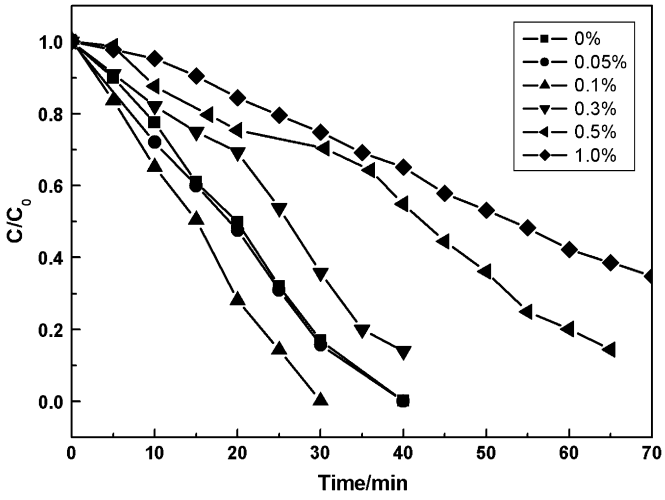

Fig. 6. Degradation profiles for $Zn/TiO_{2\ ste}$ nanocrystals calcined at 450 °C.

The photodegradation of the dye was also carried out (Fig. 7) using 0.1% $Zn/TiO_{2\ ste}$ nanocrystals calcined at various temperatures. The photoactivity of these nanocrystals followed the order: 450 °C > 400 °C > 500 °C > 600 °C.

To compare the photoactivity of TiO_2-based nanocrystals prepared by different methods, the photodegradation of MeO was also carried out using the commercial reference material, P25, $TiO_{2\ sol}$ and 0.1% $Zn/TiO_{2\ sol}$ (Fig. 8). In the absence of the catalysts (curve f) no observable degradation of the dye occurred. The photoactivity of $TiO_{2\ ste}$ and 0.1% $Zn/TiO_{2\ ste}$ (curves b and c) was much higher than that of $TiO_{2\ sol}$ and 0.1% $Zn/TiO_{2\ sol}$ (curves d and e). $TiO_{2\ ste}$ exhibited much higher photoactivity than $TiO_{2\ sol}$ and 0.1% $Zn/TiO_{2\ ste}$ displayed higher photoactivity than 0.1% $Zn/TiO_{2\ sol}$. This might be explained by the larger BET surface areas of the nanocrystals prepared by the stearic acid gel method. While 0.1% $Zn/TiO_{2\ sol}$ (curve e) has a smaller BET surface area than undoped $TiO_{2\ sol}$ (curve d), it showed higher photoactivity due to zinc doping. Of all the samples, the photoactivity of 0.1% $Zn/TiO_{2\ ste}$ (curve c) was highest and was even higher than that of the commercial compound, indicating that both the BET

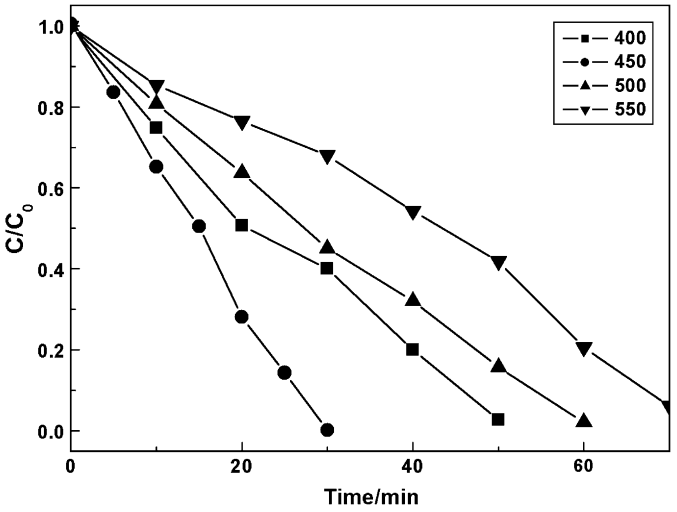

Fig. 7. Degradation profiles for 0.1% $Zn/TiO_{2\ ste}$ nanocrystals calcined at various temperatures.

surface area and zinc doping should be considered in order to obtain the best photodegradation performance.

3.6. LC/MS

Mass spectra (Fig. 9) of the solutions collected at different intervals during the photodegradation process were obtained using negative ion mode. It was found that several new peaks formed when the catalytic reaction continued for 15 min (curve b), which can be ascribed to the formation of intermediates during dye photodegradation. The colour of C.I. Acid Orange 52 stems from N=N bonds, in the process of photodegradation, we observed that the colour of solution weakened gradually, implying that the N=N bonds were destructed to form some intermediates, and the intermediates may well be

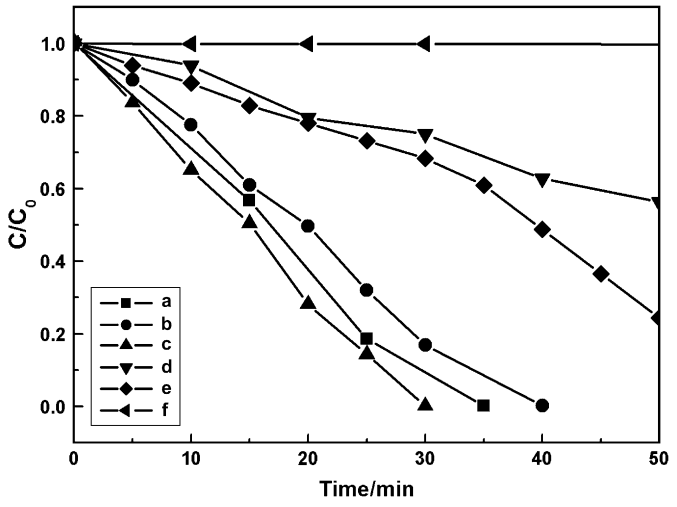

Fig. 8. Degradation profiles for TiO_2-based nanocrystals prepared by different methods: (a) P25; (b) $TiO_{2\ ste}$ calcined at 450 °C; (c) 0.1% $Zn/TiO_{2\ ste}$ calcined at 450 °C; (d) $TiO_{2\ sol}$ calcined at 450 °C; (e) 0.1% $Zn/TiO_{2\ sol}$ calcined at 450 °C; (f) blank test.

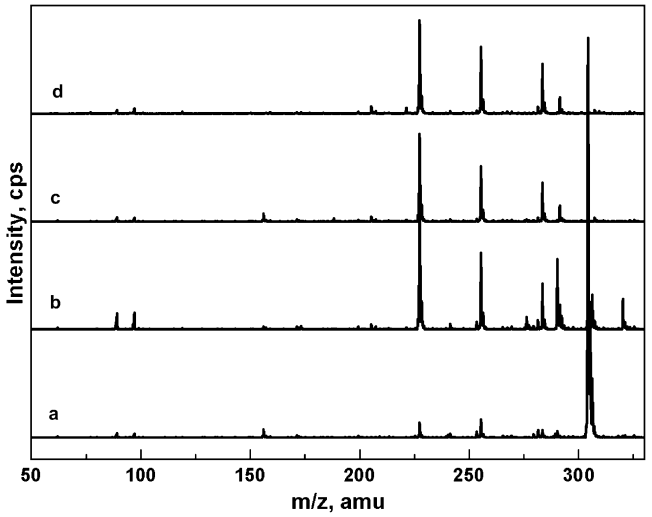

Fig. 9. Mass spectra of the solutions collected at different intervals during the degradation of 0.1% $Zn/TiO_{2\ ste}$: (a) 0 min; (b) 15 min; (c) 30 min; (d) solvent–water.

substituted aromatic degradation products. After 30 min (curve c), the peaks were the same as those for solvent–water (curve d), indicating that both the dye and the intermediates had been completely photodegraded, which indicates that the photodegradation not only destructs the conjugated system but also reduces the dye to CO_2 and H_2O.

4. Conclusions

The TiO_2-based nanocrystals prepared by the stearic acid gel method had greater BET surface area and higher photocatalytic activity. The presence of the dopant improved the photoactivity of the nanocrystals; 0.1% $Zn/TiO_{2\ ste}$ exhibited higher photoactivity than 0.1% $Zn/TiO_{2\ sol}$ and the commercial P25. A detailed explanation of these results is not easy because photoreactivity depends on the bulk, crystal phase, surface area, proportion of photoactive component, electronic property, etc. the results indicate that the surface area and the proportion of photoactive components play important roles in the photodegradation reaction.

Acknowledgements

This work was financially supported by the National Natural Science Foundation of China (60374048) and Jilin Provincial Science and Technology Department (20060928). The Authors are grateful to Lehui Zou and Lianxiang Yu for help.

References

[1] Weber EJ, Stickney VC. Hydrolysis kinetics of reactive blue 19-vinyl sulfone. Water Res 1993;27:63–7.
[2] Guettaï N, Amar HA. Photocatalytic oxidation of methyl orange in presence of titanium dioxide in aqueous suspension. Part I: parametric study. Desalination 2005;185:427–37.
[3] Saquib M, Muneer M. Titanium dioxide mediated photocatalyzed degradation of a textile dye derivative, acid orange 8, in aqueous suspensions. Desalination 2003;155:255–63;

Qamar M, Saquib M, Muneer M. Titanium dioxide mediated photocatalytic degradation of two selected azo dye derivatives, chrysoidine R and acid red 29 (chromotrope 2R), in aqueous suspensions. Desalination 2005;186:255–71.

[4] Vinodgopal K, Bedja I, Hotchandani S, Kamat PV. A photocatalytic approach for the reductive decolorization of textile azo dyes in colloidal semiconductor suspensions. Langmuir 1994;10:1767–71.

[5] Vinodgopal K, Kamat PV. Photochemistry of textile azo dyes. Spectral characterization of excited state, reduced and oxidized forms of acid orange 7. J Photochem Photobiol A 1994;83:141–6.

[6] Mills A, Belghazi A, Davies RH, Worsley D, Morris S. A kinetic study of the bleaching of rhodamine 6G photosensitized by titanium dioxide. J Photochem Photobiol A 1994;79:131–9.

[7] Vautier M, Guillard C, Herrmann JM. Photocatalytic degradation of dyes in water: case study of indigo and of indigo carmine. J Catal 2001;201:46–59.

[8] Arslan İ, Balcioğlu IA, Bahnemann DW. Advanced chemical oxidation of reactive dyes in simulated dyehouse effluents by ferrioxalate-Fenton/UV-A and TiO_2/UV-A processes. Dyes Pigments 2000;47:207–18.

[9] Sakthivel S, Neppolian B, Arabindoo B, Palanichamy M, Murugesan V. ZnO/UV mediated photocatalytic degradation of acid green 16, a commonly used leather dye. Indian J Eng Mater Sci 2000;7:87–93.

[10] Zhao JC, Wu TX, Wu KQ, Oikawa K, Hidaka H, Serpone N. Photoassisted degradation of dye pollutants. 3. Degradation of the cationic dye rhodamine B in aqueous anionic surfactant/TiO_2 dispersions under visible light irradiation: evidence for the need of substrate adsorption on TiO_2 particles. Environ Sci Technol 1998;32:2394–400.

[11] Choi WY, Termin A, Hoffmann MR. The role of metal dopants in quantum-sized TiO_2: correlation between photoreactivity and charge carrier recombination dynamics. J Phys Chem 1994;98:13669–79.

[12] Xie YB, Yuan CW. Characterization and photocatalysis of Eu^{3+}–TiO_2 sol in the hydrosol reaction system. Mater Res Bull 2004;39:533–43.

[13] Gerischer H, Heller A. The role of oxygen in photooxidation of organic molecules on semiconductor particles. J Phys Chem 1991;95:5261–7.

[14] Ohtani B, Iwai K, Nishimoto S, Sato S. Role of platinum deposits on titanium(IV) oxide particles: structural and kinetic analyses of photocatalytic reaction in aqueous alcohol and amino acid solutions. J Phys Chem B 1997;101:3349–59.

[15] Gao YM, Lee W, Trehan R, Kershaw R, Dwight K, Wold A. Improvement of photocatalytic activity of titanium(IV) oxide by dispersion of Au on TiO_2. Mater Res Bull 1991;26:1247–54.

[16] San N, Hatipoglu A, Kocturk G, Cinar Z. Photocatalytic degradation of 4-nitrophenol in aqueous TiO_2 suspensions: theoretical prediction of the intermediates. J Photochem Photobiol A 2002;146:189–97.

[17] Siemon U, Bahnemann D, Testa JJ, Rodriguez D, Litter MI, Bruno N. Heterogeneous photocatalytic reactions comparing TiO_2 and Pt/TiO_2. J Photochem Photobiol A 2002;148:247–55.

[18] Sivalingam G, Nagaveni K, Hegde MS, Madras G. Photocatalytic degradation of various dyes by combustion synthesized nano anatase TiO_2. Appl Catal B 2003;45:23–38;
Nagaveni K, Hegde MS, Madras G. Structure and photocatalytic activity of $Ti_{1-x}M_xO_{2\pm\delta}$ (M = W, V, Ce, Zr, Fe, and Cu) synthesized by solution combustion method. J Phys Chem B 2004;108:20204–12.

[19] Kasuga T, Hiramatsu M, Hoson A, Sekino T, Niihara K. Formation of titanium oxide nanotube. Langmuir 1998;14:3160–3;
Kasuga T, Hiramatsu M, Hoson A, Sekino T, Niihara K. Titania nanotubes prepared by chemical processing. Adv Mater 1999;11:1307–11.

[20] Marcì G, Augugliaro V, López-Muñoz MJ, Martín C, Palmisano L, Rives V, et al. Preparation characterization and photocatalytic activity of polycrystalline ZnO/TiO_2 systems. 1. Surface and bulk characterization. J Phys Chem B 2001;105:1026–32;
Marcì G, Augugliaro V, López-Muñoz MJ, Martín C, Palmisano L, Rives V, et al. Preparation characterization and photocatalytic activity of polycrystalline ZnO/TiO_2 systems. 2. Surface, bulk characterization, and 4-nitrophenol photodegradation in liquid–solid regime. J Phys Chem B 2001;105:1033–40.

[21] Jing LQ, Sun XJ, Cai WM, Xu ZL, Du YG, Fu HG. The preparation and characterization of nanoparticle TiO_2/Ti films and their photocatalytic activity. J Phys Chem Solids 2003;64:615–23.

[22] Akhtar MK, Vemury S, Pratsinis SE. The role of electrolytes during aerosol synthesis of TiO_2. Nanostruct Mater 1994;4:537–44.

[23] Yin HB, Wada Y, Kitamura T, Kambe S, Murasawa S, Mori H, et al. Hydrothermal synthesis of nanosized anatase and rutile TiO_2 using amorphous phase TiO_2. J Mater Chem 2001;11:1694–703.

[24] Grätzel M, Howe RF. Electron paramagnetic resonance studies of doped TiO_2 colloids. J Phys Chem 1990;94:2566–72.

[25] Jaeger CD, Bard AJ. Spin trapping and electron spin resonance detection of radical intermediates in the photodecomposition of water at TiO_2 particulate systems. J Phys Chem 1979;83:3146–52.

[26] Memming R. Solar energy conversion by photoelectrochemical processes. Electrochim Acta 1980;25:77–88.

[27] Schoonen MAA, Xu Y, Strongin DR. An introduction to geocatalysis. J Geochem Explor 1998;62:201–15.